Cobalt borophosphate on nickel foam as an electrocatalyst for water splitting

Emine Ülker [a,*], Sina Sadigh Akbari [b], Ferdi Karadas [b,c,**]

[a] Department of Chemistry, Faculty of Arts & Sciences, Recep Tayyip Erdogan University, 53100, Rize, Turkey
[b] Department of Chemistry, Bilkent University, 06800, Ankara, Turkey
[c] UNAM-Institute of Materials Science and Nanotechnology, Bilkent University, 06800, Ankara, Turkey

HIGHLIGHTS

- Cobalt borophosphate was synthesized by solid-state reaction.
- Obtained Co_3BPO_7 was used as electrocatalysts for oxygen evolution and hydrogen evolution in alkaline medium.
- Co_3BPO_7 displays high electrocatalytic performance towards OER with overpotential of 230 mV for 10 mA cm^{-2}.

ARTICLE INFO

ABSTRACT

One of the most critical steps in the transition to carbon-free energy systems is sustainable hydrogen evolution from water. In this research, a cobalt borophosphate crystalline compound consisting of phosphate and borate anions was synthesized with a solid-state reaction. X-ray diffraction (XRD), Fourier transform infrared spectroscopy (FT-IR), scanning electron microscopy (SEM), and X-ray Photoelectron (XPS) was employed to investigate the structure, composition, and morphology of Co_3BPO_7. Electrocatalytic performances of the catalyst towards oxygen evolution reaction (OER) and hydrogen evolution reaction (HER) have been investigated on nickel foam (NF) electrode in 1.0 M KOH (pH 13.6) by linear sweep voltammetry, chronopotentiometry, cyclic voltammetry, and electrochemical impedance spectroscopy. For OER, the catalyst exhibits an overpotential of 230 mV at 10 mA cm^{-2} with a Tafel slope of 130 mV dec^{-1}, which is comparable to that of the benchmark RuO_2 electrocatalyst, and 220 mV overpotential for a current density of 10 mA cm^{-2} with a Tafel slope of 147 mV dec^{-1} for HER process. Long-term chronoamperometry and multiple cyclic voltammetric experiments indicate the catalyst is stable throughout both HER and OER processes. Electrochemical experiments and characterization studies performed on the pristine and post-catalytic electrode indicate that the catalyst is robust under alkaline electrocatalytic conditions (pH 13.6).

1. Introduction

The growing energy demand due to the decreasing fossil fuel reserves and increased environmental awareness have forced scientists to find sustainable new resources with low cost and low greenhouse emissions [1]. Hydrogen is considered one of the most promising options for addressing energy shortages and environmental pollution [2,3]. This reasonable forecast is based on hydrogen-based fuel advantages of high calorific value, nontoxicity, and cleanness [4]. Hydrogen economy, where hydrogen is employed as an energy carrier, and solar energy are among the foremost alternative energy candidates as they are environmentally friendly energy sources [5]. The cheap and large-scale production of hydrogen and the sustainability of the production are the main conditions of the hydrogen economy. Although hydrogen can be produced in various processes, today about 95% of the total hydrogen production is based on fossil fuels [6]. However, electrochemical water splitting is more appealing than other technologies (such as steam methane reforming, biomass conversion, and coal gasification) because it not only uses water as a natural carrier of hydrogen but also uses electricity for carbon-free energy sources [4]. Therefore electrocatalytic

---

water splitting is considered one of the most promising approaches for converting solar energy to clean chemical fuel [5,7]. The hydrogen evolution reaction (HER) and the oxygen evolution reaction (OER) are the two half electrode processes of water splitting. Among them, OER is the main limiting process due to the sluggish reaction with poor catalytic efficiency [8]. Therefore, the development of robust, efficient, and cost-effective water oxidation catalysts is required. For efficient water oxidation catalysis, various catalysts have been investigated. Though IrO_2 and RuO_2 are identified as efficient and high activity catalysts for OER, their rarity, alkaline instability and expensiveness are their major disadvantages [9]. The main focus has been devoted to constructing electrocatalysts containing earth-abundant 3D metal ions (especially Co, Ni, Mn, and Fe) [10,11]. In this line of research, many earth-abundant compounds have been studied for efficient water oxidation catalysts such as transition metal oxides [12,13], phosphates [14], and borates [15,16]. Catalysts including nickel and cobalt prepared through electrodeposition of metal salts with borate (Bi) and phosphate (Pi) have been regarded as a significant class of efficient and low-cost electrocatalysts [17–19]. Metal borophosphates (BPOs) are well-known for their intriguing structural designs, which result from their capacity to combine borate (BO_4/BO_3) and phosphate (PO_4) units via P–O–B linkages, resulting in a wide range of connection patterns and anionic partial structure extension. The variety of boron and phosphorus atoms linked to oxygen has resulted in the creation of novel compounds with a variety of anionic partial structures. Although most of the borophosphate compounds were obtained hydrothermally, anhydrous borophosphates were obtained by the high-temperature solid-state synthesis method [20]. BPOs are intermediate compounds of the M_xO_y-B_2O_3-P_2O_5-(H_2O) systems, which consist of intricate anionic structures interlinked by trigonal-planar BO_3 and/or BO_4 and PO_4 groups, as well as their partly protonated species [21]. Although the optical [22] and thermal [23] properties of borophosphates have been studied extensively, studies on the potential of borophosphate in the field of energy conversion and storage are limited. The first study on the bifunctional electrocatalytic activities of BPOs toward water splitting involves the utilization of helical cobalt borophosphates [24]. A hydrothermally synthesized crystalline cobalt BPO ($H_{0.5}Co_{1.25}(H_2O)_{1.5}[BP_2O_8].H_2O$) [5], an amorphous N-doped cobalt BPO [25] and a manganese BPO [26] have also been investigated as efficient and durable OER electrocatalyst.

Given the promising results on BPOs, here in this study, we aimed to prepare an active BPO on a Ni foam (NF) substrate. We investigated the electrocatalytic activity of solid-state synthesized crystalline Co_3BPO_7 coated NF electrode (symbolized as [Co_3BPO_7/NF]) for water reduction and water oxidation reactions in alkaline solution (pH 13.6). Comprehensive characterization studies and electrochemical studies are performed to investigate its structural and catalytic properties.

2. Experimental section

2.1. Chemicals

All substances, including cobalt carbonate hydrate ($CoCO_3.xH_2O$), boric acid (H_3BO_3, >99.0%), ammonium dihydrogen phosphate ($(NH_4)_2HPO_4$, >99.0%), potassium dihydrogen phosphate (KH_2PO_4, purity >99.0%), dipotassium hydrogen phosphate (K_2HPO_4, purity >99.0%), potassium hydroxide (KOH, purity >99.0%), nickel foam and solvents were supplied from Merck or Aldrich and used without additional purification.

2.2. Equipments

Fourier transform infrared (FT-IR) spectra were taken by PerkinElmer Spectrum 100 spectrometer in wavenumber range between 4000 and 600 cm^{-1}. The Rigaku SmartLab X-Ray Diffractometer was used to measure X-ray diffraction (XRD) patterns. The diffraction patterns were recorded within the range of 10–80°. The Rigaku Jeol JSM-6610 was

used for scanning electron microscopy (SEM) imaging and energy-dispersive X-ray spectrum (EDS) was recorded using Oxford Instruments 51-Add0013. X-ray photoelectron (XPS) measurements were conducted by using a Thermo Scientific K-Alpha X-Ray Photoelectron Spectrometer system equipped with an AlK_α micro-focused monochromator source. The catalyst-loaded nickel foam electrodes were fixed on the sample holder for XPS measurements. All spectra were obtained using the aluminum anode (Al K_α = 1486.6 eV), which operates at a 400 μm spot size. A low-energy flood gun was used as a charge neutralizer during all experiments. The survey spectrum was recorded with a pass energy of 200 eV and a step size of 1 eV. For the high-resolution spectra, pass energy of 30 eV was used with a step size of 0.1 eV. The Gamry Instrument Interface 1000 Potentiostat/Galvanostat was used to perform all electrochemical measurements at room temperature. A standard three-electrode cell was employed, with Ag/AgCl (saturated KCl) as the reference electrode, a Pt foil as the counter electrode, and a catalyst-loaded nickel foam as the working electrode. All potentials were recorded vs. an Ag/AgCl reference electrode and then expressed vs. a reversible hydrogen electrode (RHE) by using the formula of $E_{(RHE)} = E_{(Ag/AgCl)} + 0.197 + (0.059 \times pH)$.

2.3. Synthesis of Co_3BPO_7

The compound was synthesized by solid-state reaction with a little modification of the described procedure in the literature [27]. Briefly, a mixture of $CoCO_3.xH_2O$, $(NH_4)_2HPO_4$, and H_3BO_3 in the molar ratio of 3:1:1 was grounded homogeneously in a mortar. Then, the mixture was heated in an alumina crucible to 450 °C with an increase of 15 °C per minute to the decomposition of the starting reagents and removed the volatile products such as NH_3, NO_2, CO_2, and H_2O, only the oxides remain. After being kept for 3 h at 450 °C, the mixture was taken out from the oven and again grounded to make it more homogeneous. The temperature was raised to 600 °C with a rise of 1 °C per minute, and the sample was kept for 3 h at this temperature. Then, the temperature was raised to 1050 °C with an increase of 1 °C per minute and was held for 24 h at 1050 °C. Eventually, the catalyst was slowly cooled with a decrease of 3 °C per minute to room temperature to get good crystallinity. Purple-colored product was obtained and rinsed with distilled water and ethanol before being vacuum-dried.

2.4. Preparation of modified electrodes

A piece of nickel foam (1 cm × 2 cm) was washed by sonication for 10 min in 3 M HCl, deionized water, and ethanol, respectively. Catalyst-modified electrodes were prepared by the drop-casting method. A mixture of 4 mg of catalyst, 900 μL ethanol, and 100 μL Nafion (5 wt %) solution was mixed and sonicated for 60 min to obtain a stable suspension. Then, 50 μL of the sonicated suspension of the catalyst was dropped onto a clean NF electrode (1 cm^2). The electrode was then dried in an oven at 70 °C for 10 min. This process was repeated three times. Prepared electrodes were annealed at 150 °C for 1 h, and then, they were left under vacuum in a desiccator for further electrochemical experiments. For comparison, 4 mg RuO_2 or Pt/C catalyst was dispersed in the mixture of 900 μL ethanol and 100 μL Nafion solution, followed by sonication to obtain the homogeneous ink dispersion, which was dropped onto Ni foam for OER and HER studies, respectively.

2.5. Electrochemical studies

Linear sweep voltammograms (LSVs) with a scan rate of 5 mV s^{-1} in 1 M KOH solution (pH 13.6) were used to investigate the electrocatalytic activity of the Co_3BPO_7 sample. Millipore Milli-Q water with a resistivity of 18.2 MΩ cm was used for all solutions. The scan rate was changed between 20 and 200 mV s^{-1} within the potential range between 0.6 V and 0.9 V (vs. RHE) for double-layer capacitance (C_{dl}) estimation without any Faradaic current. The difference in anodic and cathodic

current density ($\Delta j = j_a - j_c$) vs. scan rates was plotted at 0.75 V, with the slope twice that of C_{dl}. Chronopotentiometric (CP) studies were carried out in an alkaline medium with a constant current density of 10 mA cm^{-2}.

Tafel plots are derived from LSV curves to evaluate the catalytic kinetics of the Co$_3$BPO$_7$/NF sample. To calculate the Tafel slope, the logarithm of the current densities was plotted versus overpotential ($\eta = a + b \log (j)$). Tafel slope (b) was obtained from the linear region of the Tafel plot. The electrochemical impedance spectroscopy (EIS) was conducted for the Co$_3$BPO$_7$/NF and bare NF electrodes at 1.55 V (vs. RHE) after a 5-min conditioning period to obtain the Nyquist plots. Furthermore, the variation of charge transfer as a function of applied potentials (at 1.45 V–1.60 V vs. RHE) for Co$_3$BPO$_7$/NF was also evaluated. The measurements were carried out in a KOH solution (pH 13.6) with an alternating current (AC) perturbation of 5.0 mV over the frequency range of 0.01–100 kHz in 1 M KOH solution. All experiments were performed under a nitrogen atmosphere.

3. Results and discussion

3.1. Characterization studies

The crystal structure of the prepared cobalt borophosphate (Fig. 1A, PDF card: 1511069 [20]) confirmed by powder XRD of the compound (Fig. 1B) reveals that cobalt sites reside in the distorted square-pyramidal coordination spheres surrounded by BO$_3^{3-}$ and PO$_4^{3-}$ anionic groups. The unit cell of the compound adopts a monoclinic system with the space group Cm. The structure consists of Co sites with trigonal bipyramidal, square pyramidal, and distorted octahedral geometries. Polyhedral Co centers, triangular B centers, and tetrahedral P centers are joined together to form a three-dimensional network [20]. In addition, Fig. S1 shows the effect of reaction time and temperature on the crystallinity of Co$_3$BPO$_7$. Best crystal forms were obtained at 1050 °C

for 24 h. The Infrared spectrum of the Co$_3$BPO$_7$ sample also confirms the presence of triangular planar BO$_3^{3-}$ and tetrahedral PO$_4^{3-}$ groups in the structure (Fig. S2) [28]. The IR band of the borophosphate structure reveals strong and broad stretching and bending absorption bands in the 1400-800 cm^{-1} region, which are attributed to B–O and P–O groups [29]. Furthermore, the strong P–O stretching modes in the 800–1100 cm^{-1} region overlap with the strong B–O stretching vibrations [24]. However, the bands observed at 1224 cm^{-1} (υ_3(BO$_3$)), 1027 cm^{-1} (υ_3(PO$_4$) and υ_1(BO$_3$)), 983 cm^{-1} (υ_1(PO$_4$) and υ_1(BO$_3$)), 742 and 718 cm^{-1} (υ_2(BO$_3$)) confirm the presence of (BO$_3$)$^{3-}$ and (PO$_4$)$^{3-}$ anionic groups in the structure. Besides, the absence of a band at 1150 cm^{-1} that is assigned to the B–O stretching vibration of a BO$_4$ group confirms that the boron is not tetrahedrally coordinated as expected [30]. SEM displays that Co$_3$BPO$_7$ has a hexagonal bipyramidal structure (Fig. 1C). The composition of the Co$_3$BPO$_7$ was confirmed by EDS analysis (Fig. 1D).

X-ray photoelectron spectroscopy (XPS) was performed to investigate the chemical composition of the Co$_3$BPO$_7$ electrode. In general, the Co 2p$_{1/2}$—2p$_{3/2}$ spin-orbit splitting is 15 eV and 16 eV for diamagnetic Co(III) and paramagnetic Co(II), respectively [31,32]. The Co 2p spectrum of the Co$_3$BPO$_7$ electrode exhibits two main peaks that correspond to Co 2p$_{3/2}$ (781.9 eV) and Co 2p$_{1/2}$ (797.7 eV) with shake-up satellite peaks at higher binding energies. The presence of intense satellite peaks and the 2p$_{1/2}$—2p$_{3/2}$ spin-orbit splitting of 15.8 eV suggest that the cobalt cations are mainly in a +2 oxidation state (Fig. 2A) [24,31,32]. The O 1s signal is deconvoluted into two peaks at 531 eV and 532.2 eV, which can be assigned to the P–O and B–O bonds, respectively (Fig. 2B) [33,34]. The P 2p spectrum is also divided into two peaks at 133.3 eV and 134.1 eV corresponding to P 2p$_{3/2}$ and 2p$_{1/2}$ of the phosphate group, respectively (Fig. 2C) [24]. The B 1s spectrum of the Co$_3$BPO$_7$ electrode exhibits a peak at 191.1 eV, which is assigned to the B–O bonds in the metal borate structure (Fig. 2D) [25].
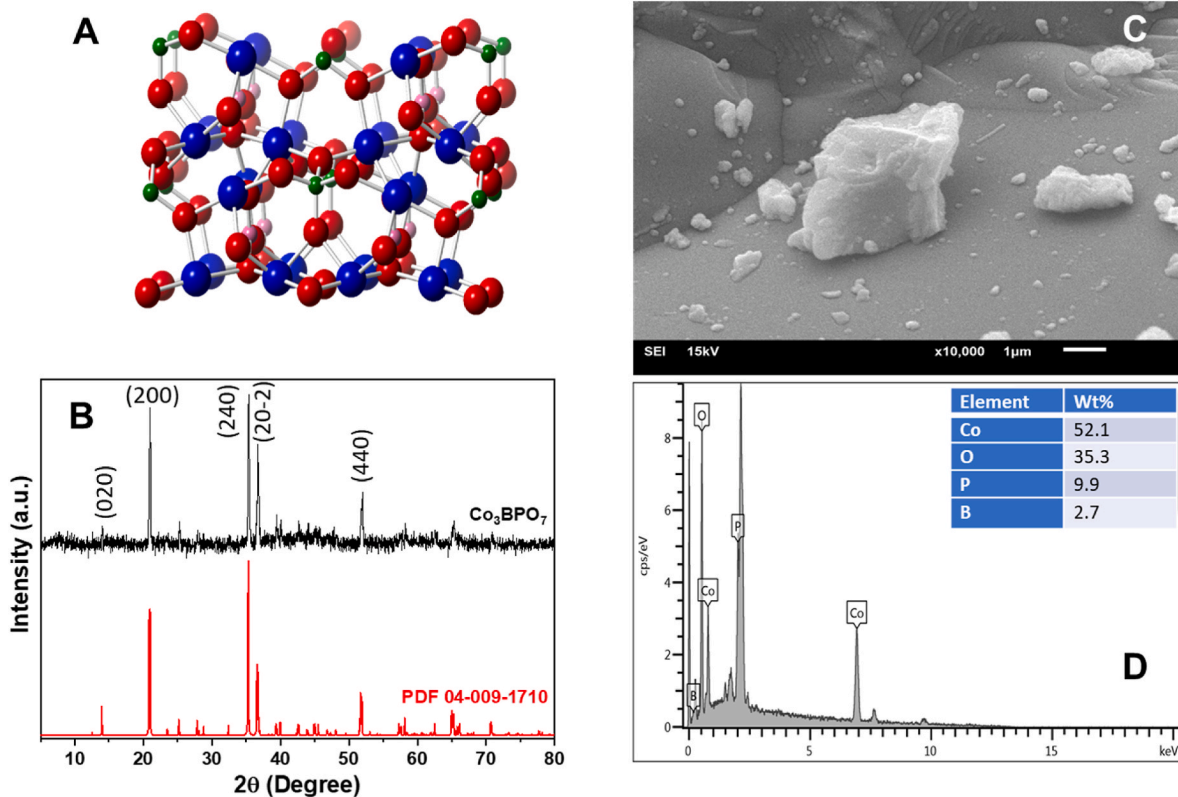

Fig. 1. A) Crystal structure (blue: cobalt, red: oxygen, green: phosphorus, pink: boron), B) XRD pattern, C) SEM image and D) EDS spectrum of Co$_3$BPO$_7$. (For interpretation of the references to color in this figure legend, the reader is referred to the Web version of this article.)
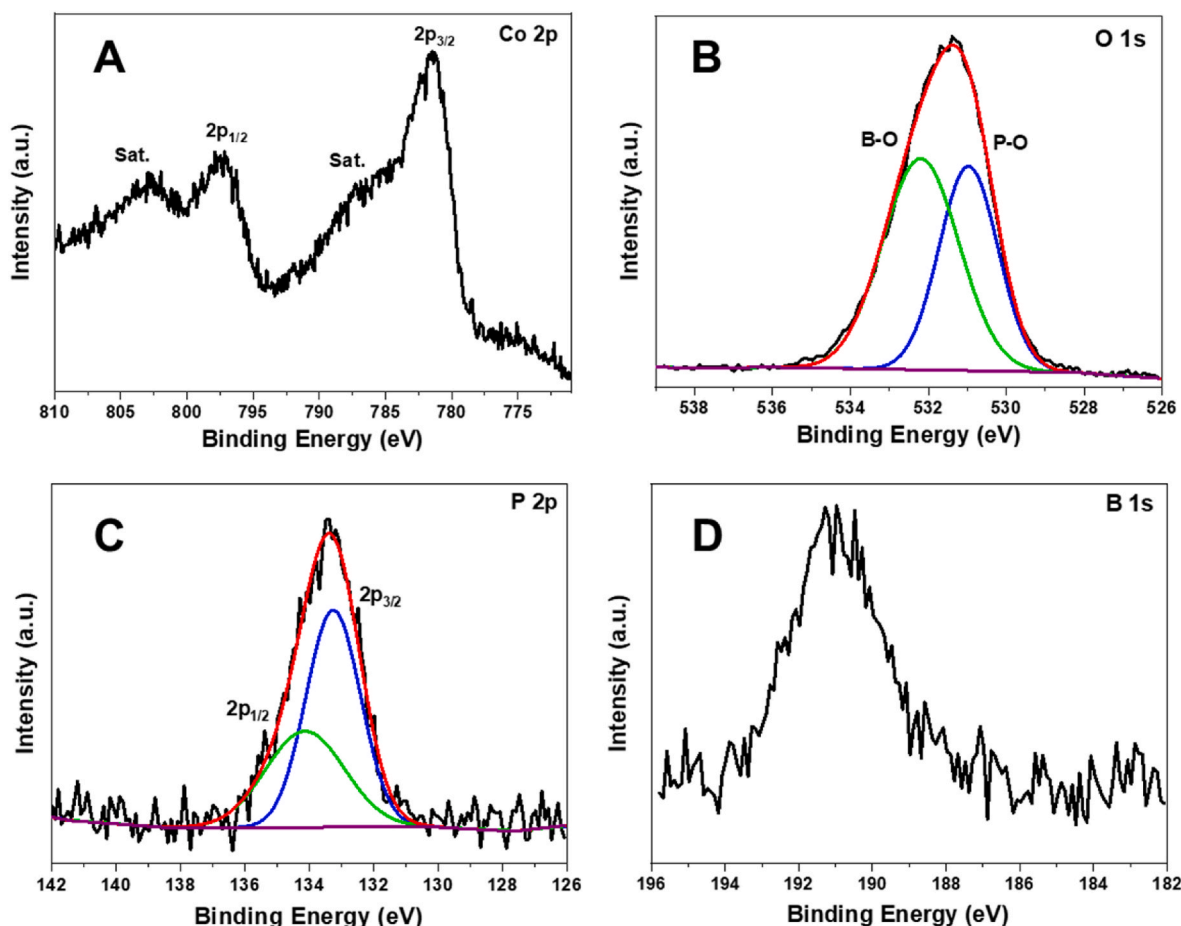
Fig. 2. XPS profiles of A) Co 2p, B) O 1s, C) P 2p, and D) B 1s signals for Co_3BPO_7.

3.2. Electrocatalytic OER and HER studies

The electrocatalytic OER performance of Co_3BPO_7 coated NF was initially evaluated by LSV experiment with a scan rate of 5 mV s^{-1} in 1 M KOH solution (Fig. 3A). RuO_2 on Ni foam was also tested for comparison. A peak at approximately 1.5 V, the common oxidation peak for the Ni$^{2+/}$ $^{3+}$ redox pair, was not observed on the LSV profile of the Co_3BPO_7/NF electrode. The bare NF has no observable activity towards OER, while Co_3BPO_7/NF sample exhibits an overpotential of 230 mV at a current density of 10 mA cm^{-2}. It is notable that, this overpotential is lower than that of the RuO_2 which is the state-of-the-art OER catalyst (Fig. 3A). The LSV obtained at a scan rate of 5 mV s^{-1} reveals a Tafel slope of 130 mV dec^{-1} when the linear plot is assumed just after the onset overpotential of 160 mV (Fig. 3B). Electrochemically active surface area (ECSA) was evaluated from double-layer capacitance (C_{dl}), which is linearly proportional to the ECSA [35]. CVs with different scan rates were recorded in a non-faradaic region where no redox activity is observed (Fig. S3). The difference in anodic and cathodic current density ($\Delta_j = j_a - j_c$) vs. scan rate was plotted at 0.75 V, with the slope twice that of C_{dl}. C_{dl} of Co_3BPO_7/NF was calculated to be 0.4 mF cm^{-2}, which is much larger than calculated for Cu_2FeSnS_4 (0.28 mF cm^{-2}, before CA) [36], for CoCo-PBA (0.15 mF cm^{-2}), CoFe PBA (0.14 mF cm^{-2}), FeFe PBA (0.07 mF cm^{-2}) and NiFe PBA (0.06 mF cm^{-2}) [37] (Fig. 3C).

The Co_3BPO_7/NF electrode stability was determined by a chronopotentiometry experiment for 10 h at 10 mA cm^{-2} current density (Fig. 3D). In an alkaline solution, the electrode exhibits an overpotential of 230 mV at a current density of 10 mA cm^{-2}. The electrocatalytic activity of Co_3BPO_7/NF is significantly higher than several crystalline systems such as Co_3O_4 (525 mV) [38], Mn_3O_4/CoSe$_2$ composite (450 mV) [39], 1P–Co@NF (320 mV) [40] and Co_3O_4/NiCo$_2O_4$ nanocages

(340 mV) [41] in alkaline solution. On the other hand, the activity is similar to the previously reported BPOs; LiCoBPO/NF (216 mV) and NaCoBPO/NF (242 mV) [24], LiMnBPO/NF (228 mV) and NaMnBPO/NF (262 mV) [26], and NCoBPi-PVP-450/GC (276 mV) [25]. The electrocatalytic performance of Co_3BPO_7 is compared to selected studies in Table S1. The stability of the electrode was evaluated by comparing LSVs before and after the CP experiment. A slight increase in the activity was observed after the CP measurement (Fig. 3E). The stability of the Co_3BPO_7/NF electrode was also investigated with multiple cyclic voltammetric experiments. The anodic current density displays a noticeable increase after 500 cycles in comparison with its initial state, which exhibits a steady profile up to 1000 cycles (Fig. 3F), confirming the result that the catalyst has high stability.

An impedance study was also carried out to further investigate the catalytic performance of the Co_3BPO_7/NF sample. Fig. 4 A-B demonstrate the Nyquist and Bode plots for Co_3BPO_7/NF at different potentials (1.45–1.60 V) in 1 M KOH solution with 5 mV AC signals in a range of 100 kHz to 0.01 Hz frequency, respectively. In addition, a comparison of Nyquist plots recorded at 1.55 V for Co_3BPO_7/NF and bare NF electrode is shown in Fig. S4. For each study case, a semi-circular loop was observed, showing that there was no mass transfer limitation in the tested potential range [42]. A lower semi-circular diameter was observed with the increase of applied DC potential, representing faster charge transfer. An equivalent circuit was used to investigate the impedance contribution from the faradaic process. The EIS data were fitted according to the literature [42,43]. The equivalent circuit shown in Fig. 4A inset is L R_{HF} ($R_{ct}C_1$) (R_1C_2), where L, R_{HF}, R_{ct}, and C_1 symbolize inductance, resistance at high frequencies, charge transfer resistance, and DL capacitance, respectively. Resistance at high frequencies arising from the bulk electrolyte solution increased slightly with the
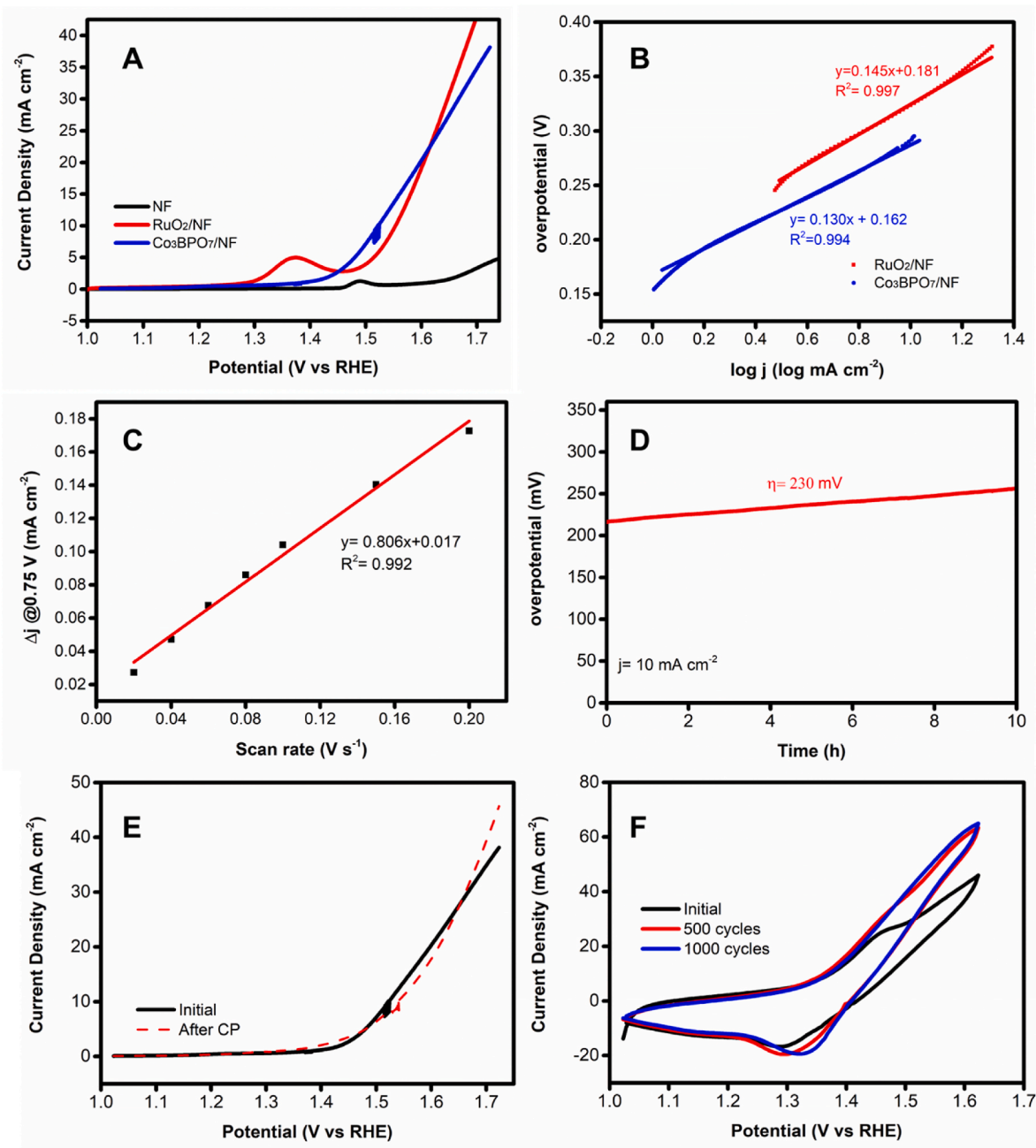
Fig. 3. A) Polarization curves of Co_3BPO_7/NF, RuO_2/NF, and blank NF electrodes for OER with a scan rate of 5 mV s^{-1}. B) Tafel plot extracted from LSV curve of Co_3BPO_7/NF and RuO_2/NF. C) Current density dependence of the scan rate at 0.75 V. The C_{dl} value is obtained as 0.4 mF cm^{-2}. D) The chronopotentiometric (CP) curve of Co_3BPO_7/NF electrode at 10 mA cm^{-2} for 10 h. E) Polarization curves recorded before and after CP measurement and F) Comparison of an initial CV of the Co_3BPO_7/NF catalyst with those after 500 and 1000 cycles.

applied potential. This is due to the formation of gas bubbles, which obstruct OH$^-$ transfer. Also, all R_{HF} were similar because the same electrolysis cell was used in all EIS measurements. The parallel (R_1C_2) circuit is derived from the dielectric properties and resistivity of the film, whereas $(R_{ct}C_1)$ is due to the Faradaic process of the OER reaction. Nyquist plots indicate that the Co_3BPO_7/NF has a smaller charge transfer resistance (4.4 Ω) compared to bare NF (14.5 Ω) at 1.55 V, which suggests that Co_3BPO_7 possesses a faster charge transfer process and has higher the intrinsic activity of electrocatalyst (Fig. S4). R_{ct}, as expected, is strongly dependent on the applied potential and decreases with increasing potential. The presence of two electrode processes is more clearly revealed in the phase angle curve of Bode plots (Fig. 4B), where the distinct characteristic frequencies of two parallel R–C circuits

can be appreciated. Table S2 lists the calculated values from impedance measurements for Co_3BPO_7 at different potentials.

We further compared the HER activity of Co_3BPO_7/NF, Pt/C, and NF under the same conditions. Fig. 5A shows the LSV recorded in 1 M KOH for the electrochemical HER performance of electrodes. As shown in Fig. 5A, the Pt/C exhibits the best performance, followed by the Co_3BPO_7/NF, which only requires a 220 mV overpotential to obtain a current density of −10 mA cm^{-2}, which this value is comparable to those of high-performance transition metal-based catalysts (Table S3). Moreover, the HER activity of Co_3BPO_7/NF is also comparable to other BPO-based catalysts such as LiCoBPO/NF (121 mV) and NaCoBPO/NF (207 mV) [24]. The HER reaction on the Co_3BPO_7/NF surface favors the Volmer–Heyrovsky mechanism, where the water discharge (Volmer

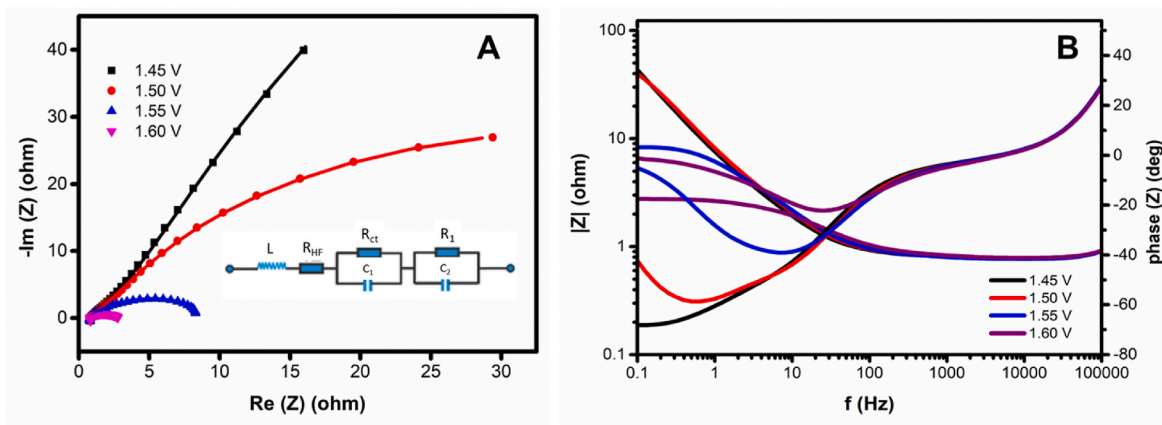**Fig. 4.** Electrochemical impedance spectroscopy (EIS) curves of Co_3BPO_7/NF at different potential A) Nyquist plot, Fit data is indicated by line, inset: proposed equivalent circuit. B) Bode plots.
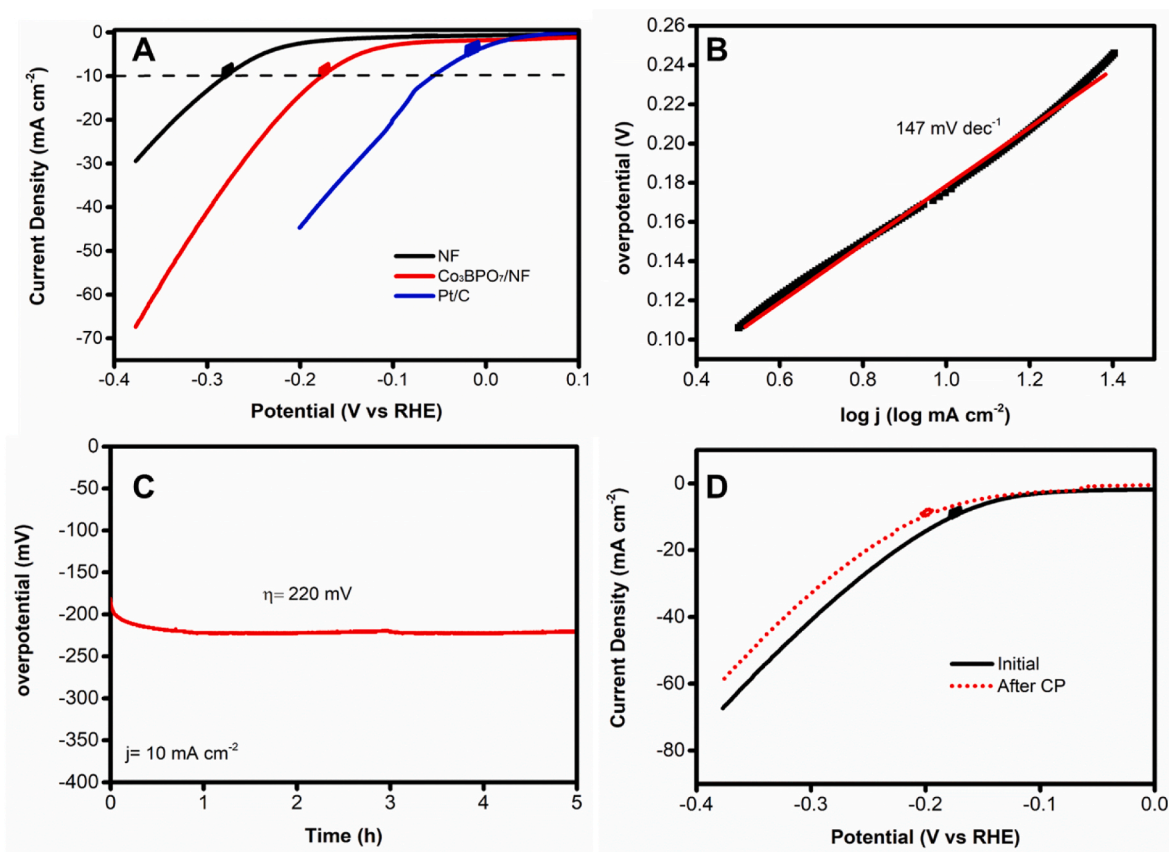

Fig. 5. A) Polarization curves of NF, Co_3BPO_7/NF, and Pt/C/NF electrodes with a scan rate of 5 mV s^{-1} for HER. B) Tafel plot of Co_3BPO_7/NF extracted from LSV curve. C) CP curve of Co_3BPO_7/NF at −10 mA cm^{-2} for 5 h. D) Polarization curves recorded before and after CP measurement.

step) reaction is the rate-limiting step according to the matching Tafel slope (140 mV dec^{-1}) (Fig. 5B) [24,44,45]. The exchange current density (j_0) is calculated as 0.53 mA cm^{-2} from the Tafel analysis at an overpotential of 0 V Co_3BPO_7/NF, thus exhibits an exchange current density higher than many noble-metal-free HER catalysts such as Ni_5P_4 NCs [46] (0.057 mA cm^{-2}) and CoP/CC [47] (0.29 mA cm^{-2}).

Similar to the OER part, the stability of Co_3BPO_7/NF during the HER process was analyzed with CP measurement at −10 mA cm^{-2} for 5 h (Fig. 5C). It acquires an overpotential of 220 mV, which stays constant during a 5 h catalytic experiment. The LSV performed before and after CP measurement was compared in Fig. 5D. A slight decrease in the

current density observed from the LSV is attributed to the mechanical removal of the catalyst from the electrode surface. In addition, there is no significant change in Co 2p XPS profile in pristine and post-catalytic samples (Fig. S5). SEM images of the as-prepared and the after CP materials reveal no changes on the surface of the Co_3BPO_7 crystallites (Fig. S6). These results suggest that the Co_3BPO_7 structure is stable during the electrocatalytic reaction.

When compared to the bifunctional electrodes in the literature, the Co_3BPO_7/NF electrode exhibits a promising bifunctional electrocatalytic performance. The Co_3BPO_7/NF electrode, in particular, can achieve j_{10} at a lower overpotential (230 mV) than the core-shell-shaped

Fe–Co$_3$O$_4$ grown on carbon nanotubes (Fe–Co$_3$O$_4$/CNTs) (300 mV) catalyst, which is synthesized by a simple chemical method [48], FeNi$_3$ and NiFe$_2$O$_4$ embedded in an N-doped carbon-carbon nanotube matrix (Fe–Ni@NC-CNTs) (274 mV) [49] and 2D Co$_2$P@Co$_3$O$_4$ (393 mV) nanohybrids through a topotactic conversion reaction, based on the surface corrosion of hexagonal single-crystal β-Co(OH)$_2$ platelets with NaH$_2$PO$_2$ [50]. For HER performance, the Co$_3$BPO$_7$/NF electrode can achieve j$_{-10}$ at a reasonable overpotential (220 mV) to that of the Fe–Co$_3$O$_4$/CNTs (140 mV) [48], Fe–Ni@NC-CNTs (202 mV) [49] and Co$_2$P@Co$_3$O$_4$ (159 mV) [50].

4. Conclusions

In summary, a crystalline cobalt borophosphate has been synthesized and evaluated as an electrocatalyst for OER and HER processes. Co$_3$BPO$_7$/NF exhibits an electrocatalytic performance with an overpotential of 230 mV and 220 mV at 10 mA cm^{-2} and -10 mA cm^{-2}, respectively, under alkaline conditions. The electrocatalytic activity could be attributed to its 3D zeolite-like structure, which can boost active site density and, thus, support mass transportation. The enhancement could be attributed to the relatively high activity of cobalt sites in the borophosphate structure. Tetrahedral phosphate groups and triangular planar borate groups could be providing an ideal platform for cobalt sites to easily change their oxidation state without going through a possible decomposition pathway. Additionally, at a current density of 10 mA cm^{-2}, the cobalt borophosphate electrode could maintain its stability for over 10 h. For HER, an exchange current density of 0.53 mA cm^{-2} is obtained. Since the expected properties of the electrocatalysts are low overvoltage, high exchange current density, and high stability, Co$_3$BPO$_7$/NF has the potential to satisfy the conditions of an ideal electrocatalyst for water splitting.

CRediT authorship contribution statement

Emine Ülker: Conceptualization, Investigation, Writing – original draft, Project administration, Funding acquisition. **Sina Sadigh Akbari:** XPS measurements and data analysis, Writing – original draft, Investigation. **Ferdi Karadas:** Conceptualization, Writing – original draft, Project administration.

Declaration of competing interest

The authors declare that they have no known competing financial interests or personal relationships that could have appeared to influence the work reported in this paper.

Acknowledgement

Appendix A. Supplementary data

Supplementary data to this article can be found online at https://doi.org/10.1016/j.matchemphys.2022.126390.

References

[1] R. Boppella, J. Tan, J. Yun, S.V. Manorama, J. Moon, Anion-mediated transition metal electrocatalysts for efficient water electrolysis : recent advances and future perspectives, Coord. Chem. Rev. 427 (2021), 213552, https://doi.org/10.1016/j.ccr.2020.213552.

[2] A.A. Hameed, M.A. Alheety, A.R. Mahmood, S.A. Al-Jibori, A. Karadag, H2 storage abilities of some novel Pd(II) complexes containing 2H[1,4]benzothiazin-3(4H)-one, Inorg. Chem. Commun. 106 (2019) 11–17, https://doi.org/10.1016/j.inoche.2019.05.012.

[3] S.A. Al-Jibori, M.M. Amen, M.A. Alheety, A. Karadag, C. Wagner, Hydrogen storage capacity of novel mixed ligand complexes of lead(II): molecular structure of [Pb2 (tsac)4(μ-dppe)], Inorg. Chem. Commun. 125 (2021), 108444, https://doi.org/10.1016/j.inoche.2021.108444.

[4] Y. Xu, C. Wang, Y. Huang, J. Fu, Recent advances in electrocatalysts for neutral and large-current-density water electrolysis, Nano Energy 80 (2021), 105545, https://doi.org/10.1016/j.nanoen.2020.105545.

[5] E. Ülker, Hydrothermally synthesized cobalt borophosphate as an electrocatalyst for water oxidation in the pH range from 7 to 14, Chemelectrochem 6 (2019) 3132–3138, https://doi.org/10.1002/celc.201900683.

[6] K.H. Ng, S.Y. Lai, C.K. Cheng, Y.W. Cheng, C.C. Chong, Photocatalytic water splitting for solving energy crisis: myth, Fact or Busted? Chem. Eng. J. 417 (2021), 128847 https://doi.org/10.1016/j.cej.2021.128847.

[7] Y. Li, X. Du, J. Huang, C. Wu, Y. Sun, G. Zou, C. Yang, J. Xiong, Recent progress on surface reconstruction of earth-abundant electrocatalysts for water oxidation, Small 15 (2019) 1–18, https://doi.org/10.1002/smll.201901980.

[8] H. Zhou, F. Yu, J. Sun, R. He, S. Chen, C. Chu, Z. Ren, Highly active catalyst derived from a 3D foam of Fe (PO 3) 2/Ni 2 P for extremely efficient water oxidation, Proc. Natl. Acad. Sci. USA 114 (2017) 5607–5611, https://doi.org/10.1073/pnas.1701562114.

[9] Y. Lee, J. Suntivich, K.J. May, E.E. Perry, Y. Shao-Horn, Synthesis and activities of rutile IrO 2 and RuO 2 nanoparticles for oxygen evolution in acid and alkaline solutions, J. Phys. Chem. Lett. 3 (2012) 399–404, https://doi.org/10.1021/jz2016507.

[10] G. Mattioli, P. Giannozzi, A. Amore Bonapasta, L. Guidoni, Reaction pathways for oxygen evolution promoted by cobalt catalyst, J. Am. Chem. Soc. 135 (2013) 15353–15363, https://doi.org/10.1021/ja401797v.

[11] K. Jin, J. Park, J. Lee, K.D. Yang, G.K. Pradhan, U. Sim, D. Jeong, H.L. Jang, S. Park, D. Kim, N.-E. Sung, S.H. Kim, S. Han, K.T. Nam, Hydrated manganese(II) phosphate (Mn3(PO4)2·3H2O) as a water oxidation catalyst, J. Am. Chem. Soc. 136 (2014) 7435–7443, https://doi.org/10.1021/ja5026529.

[12] N.K. Reddy, S. Winkler, N. Koch, N. Pinna, Electrochemical water oxidation of ultrathin cobalt oxide-based catalyst supported onto aligned ZnO nanorods, ACS Appl. Mater. Interfaces 8 (2016) 3226–3232, https://doi.org/10.1021/acsami.5b10858.

[13] M. Risch, F. Ringleb, M. Kohlhoff, P. Bogdanoff, P. Chernev, I. Zaharieva, H. Dau, Water oxidation by amorphous cobalt-based oxides: in situ tracking of redox transitions and mode of catalysis, Energy Environ. Sci. 8 (2015) 661–674, https://doi.org/10.1039/c4ee03004d.

[14] H.S. Ahn, A.J. Bard, Surface interrogation of CoPi water oxidation catalyst by scanning electrochemical microscopy, J. Am. Chem. Soc. 137 (2015) 612–615, https://doi.org/10.1021/ja511740h.

[15] M. Dincă, Y. Surendranath, D.G. Nocera, Nickel-borate oxygen-evolving catalyst that functions under benign conditions, Proc. Natl. Acad. Sci. U.S.A. 107 (2010) 10337–10341, https://doi.org/10.1073/pnas.1001859107.

[16] E.A. Turhan, S.V.K. Nune, E. Ülker, U. Şahin, Y. Dede, F. Karadas, Water oxidation electrocatalysis with a cobalt-borate-based hybrid system under neutral conditions, Chem. Eur J. 24 (2018) 10372–10382, https://doi.org/10.1002/chem.201801412.

[17] Y. Surendranath, M. Dincă, D.G. Nocera, Electrolyte-dependent electrosynthesis and activity of cobalt-based water oxidation catalysts, J. Am. Chem. Soc. 131 (2009) 2615–2620, https://doi.org/10.1021/ja807769r.

[18] M.W. Kanan, D.G. Nocera, In situ formation of an oxygen-evolving catalyst in neutral water containing phosphate and Co2+, Science 321 (2008) 1072–1075, https://doi.org/10.1126/science.1162018.

[19] D.K. Bediako, B. Lassalle-Kaiser, Y. Surendranath, J. Yano, V.K. Yachandra, D. G. Nocera, Structure-activity correlation in a nickel-borate oxygen evolution catalyst, J. Am. Chem. Soc. 134 (2012) 6801–6809, https://doi.org/10.1021/ja301018q.

[20] A. Yilmaz, X. Bu, M. Kizilyalli, R. Kniep, G.D. Stucky, Cobalt borate phosphate, Co3 [BPO7], synthesis and characterization, J. Solid State Chem. 156 (2001) 281–285, https://doi.org/10.1006/jssc.2000.8963.

[21] R. Kniep, H. Engelhardt, C. Hauf, A first approach to borophosphate structural chemistry, Chem. Mater. 10 (1998) 2930–2934, https://doi.org/10.1021/cm980263g.

[22] F.H. Elbatal, S. Ibrahim, A.M. Abdelghany, Optical and FTIR spectra of NdF3-doped borophosphate glasses and effect of gamma irradiation, J. Mol. Struct. 1030 (2012) 107–112, https://doi.org/10.1016/j.molstruc.2012.02.049.

[23] D. Carta, D. Qiu, P. Guerry, I. Ahmed, E.A. Abou Neel, J.C. Knowles, M.E. Smith, R. J. Newport, The effect of composition on the structure of sodium borophosphate glasses, J. Non-Cryst. Solids 354 (2008) 3671–3677, https://doi.org/10.1016/j.jnoncrysol.2008.04.009.

[24] P.W. Menezes, A. Indra, I. Zaharieva, C. Walter, S. Loos, S. Hoffmann, R. Schlogl, H. Dau, M. Driess, Helical cobalt borophosphates to master durable overall water-splitting, Energy Environ. Sci. 12 (2019) 988–999, https://doi.org/10.1039/C8EE01669K.

[25] B. Wang, W. Lu, Z. Huang, W. Chen, J.-L. Xie, D.-S. Pan, L.-L. Zhou, J.-L. Song, Amorphous N-doped cobalt borophosphate nanoparticles as robust and durable electrocatalyst for water oxidation, ACS Sustain. Chem. Eng. 7 (2019) 13981–13988, https://doi.org/10.1021/acssuschemeng.9b02449.

[26] P.W. Menezes, C. Walter, B. Chakraborty, J.N. Hausmann, I. Zaharieva, A. Frick, E. Von Hauff, H. Dau, M. Driess, Combination of highly efficient electrocatalytic water oxidation with selective oxygenation of organic substrates using manganese borophosphates, Adv. Mater. 33 (2021), 2004098, https://doi.org/10.1002/adma.202004098.

[27] B. Tekin, H. Güler, Synthesis and crystal structure of dicobalt nickel orthoborate, Co2Ni(BO3)2, Mater. Chem. Phys. 108 (2008) 88–91, https://doi.org/10.1016/j.matchemphys.2007.09.008.

[28] L.I. Hong-Rui, Synthesis and crystal structure of a novel borophosphate compound with noncentrosymmetric:Cd3BPO7, Chinese, J. Struct. Chem. 33 (2014) 209–215.

[29] R.P. Bontchev, S.C. Sevov, Co(5)BP(3)O(14): the first borophosphate with planar BO(3) groups connected to PO(4) tetrahedra, Inorg. Chem. 35 (1996) 6910–6911. http://www.ncbi.nlm.nih.gov/pubmed/11666863.

[30] A. Osaka, K. Takahashi, M. Ikeda, Infrared study of trivalent cations B and Fe in amorphous and crystalline phosphates, J. Mater. Sci. Lett. 3 (1984) 36–38, https://doi.org/10.1007/BF00720069.

[31] H. Haraguchi, K. Fujiwara, F. Keiichiro, A study of cobalt complexes by X-ray photoelectron spectroscopy, Chem. Lett. 4 (1975) 409–414.

[32] D. Briggs, V.A. Gibson, Direct observation of multiplet splitting in 2P photoelectron peaks of cobalt complexes, Chem. Phys. Lett. 25 (1974) 493–496, https://doi.org/10.1016/0009-2614(74)85350-9.

[33] M. Pramanik, C. Li, M. Imura, V. Malgras, Y.M. Kang, Y. Yamauchi, Ordered mesoporous cobalt phosphate with crystallized walls toward highly active water oxidation electrocatalysts, Small 12 (2016) 1709–1715, https://doi.org/10.1002/smll.201503187.

[34] X. Sun, Y. Ding, B. Zhang, R. Huang, D.S. Su, New insights into the oxidative dehydrogenation of propane on borate-modified nanodiamond, Chem. Commun. 51 (2015) 9145–9148, https://doi.org/10.1039/c5cc00588d.

[35] Q. Hu, X. Liu, C. Tang, L. Fan, Facile fabrication of a 3D network composed of N-doped carbon-coated core–shell metal oxides/phosphides for highly efficient water splitting, Sustain. Energy Fuels 2 (2018) 1085–1092, https://doi.org/10.1039/C7SE00576H.

[36] J.N. Hausmann, E.M. Heppke, R. Beltrán-Suito, J. Schmidt, M. Mühlbauer, M. Lerch, P.W. Menezes, M. Driess, Stannites – a new promising class of durable electrocatalysts for efficient water oxidation, ChemCatChem 12 (2020) 1161–1168, https://doi.org/10.1002/cctc.201901705.

[37] W. Sun, Z. Wei, J. Qi, L. Kang, J. Li, J. Xie, B. Tang, Y. Xie, Rapid and scalable synthesis of prussian blue analogue nanocubes for electrocatalytic water oxidation, Chin. J. Chem. 39 (2021) 2347–2353, https://doi.org/10.1002/cjoc.202100294.

[38] H. Tüysüz, Y.J. Hwang, S.B. Khan, A.M. Asiri, P. Yang, Mesoporous Co3O4 as an electrocatalyst for water oxidation, Nano Res. 6 (2013) 47–54, https://doi.org/10.1007/s12274-012-0280-8.

[39] M.-R. Gao, Y.-F. Xu, J. Jiang, Y.-R. Zheng, S.-H. Yu, Water oxidation electrocatalyzed by an efficient Mn3O4/CoSe2 nanocomposite, J. Am. Chem. Soc. 134 (2012) 2930–2933, https://doi.org/10.1021/ja211526y.

[40] K. Li, T. zhen Ren, Z.Y. Yuan, T.J. Bandosz, Electrodeposited P–Co nanoparticles in deep eutectic solvents and their performance in water splitting, Int. J. Hydrogen Energy 43 (2018) 10448–10457, https://doi.org/10.1016/j.ijhydene.2018.04.136.

[41] H. Hu, B. Guan, B. Xia, X.W. (David) Lou, Designed formation of Co3O4/NiCo2O4 double-shelled nanocages with enhanced pseudocapacitive and electrocatalytic properties, J. Am. Chem. Soc. 137 (2015) 5590–5595, https://doi.org/10.1021/jacs.5b02465.

[42] G. Li, L. Anderson, Y. Chen, M. Pan, P.Y. Abel Chuang, New insights into evaluating catalyst activity and stability for oxygen evolution reactions in alkaline media, Sustain. Energy Fuels 2 (2018) 237–251, https://doi.org/10.1039/c7se00337d.

[43] N.J. Pérez-Viramontes, V.H. Collins-Martínez, I.L. Escalante-García, J.R. Flores-Hernández, M. Galván-Valencia, S.M. Durón-Torres, Ir-Sn-Sb-O electrocatalyst for oxygen evolution reaction: physicochemical characterization and performance in water electrolysis single cell with solid polymer electrolyte, Catalysts 10 (2020), https://doi.org/10.3390/catal10050524.

[44] E.P. Alsaç, E. Ulker, S.V.K. Nune, F. Karadas, A cyanide-based coordination polymer for hydrogen evolution electrocatalysis, Catal. Lett. 148 (2018) 531–538, https://doi.org/10.1007/s10562-017-2271-6.

[45] Z. Kap, E. Ülker, S.V.K. Nune, F. Karadas, Electrocatalytic hydrogen evolution with cobalt–poly(4-vinylpyridine) metallopolymers, J. Appl. Electrochem. 48 (2018) 201–209, https://doi.org/10.1007/s10800-018-1152-z.

[46] Y. Pan, Y. Liu, J. Zhao, K. Yang, J. Liang, D. Liu, W. Hu, D. Liu, Y. Liu, C. Liu, Monodispersed nickel phosphide nanocrystals with different phases: synthesis, characterization and electrocatalytic properties for hydrogen evolution, J. Mater. Chem. A. 3 (2015) 1656–1665, https://doi.org/10.1039/C4TA04867A.

[47] J. Tian, Q. Liu, A.M. Asiri, X. Sun, Self-supported nanoporous cobalt phosphide nanowire arrays: an efficient 3D hydrogen-evolving cathode over the wide range of pH 0-14, J. Am. Chem. Soc. 136 (2014) 7587–7590, https://doi.org/10.1021/ja503372r.

[48] H. Begum, S. Jeon, Highly efficient and stable bifunctional electrocatalyst for water splitting on Fe–Co3O4/carbon nanotubes, Int. J. Hydrogen Energy (2018), https://doi.org/10.1016/j.ijhydene.2018.01.053.

[49] A.X. Zhao, P. Pachfule, S. Li, J.R. Justin, J. Schmidt, A. Thomas, X. Zhao, P. Pachfule, S. Li, J. Ron, J. Simke, J. Schmidt, A. Thomas, Bifunctional electrocatalysts for overall water splitting from a Fe/Ni-based bimetallic metal organic framework/dicyandiamide composite, Angew. Chemie Int. Ed. (n.d.). doi: 10.1002/anie.201803136.

[50] L. Yao, N. Zhang, Y. Wang, Y. Ni, D. Yan, C. Hu, Facile formation of 2D Co2P@Co3O4 microsheets through in-situ toptactic conversion and surface corrosion: bifunctional electrocatalysts towards overall water splitting, J. Power Sources 374 (2018) 142–148, https://doi.org/10.1016/J.JPOWSOUR.2017.11.028.